

Adversarial Swarms as Dynamical Systems

Soham Gupta¹ and John Baker¹

¹*University of Alabama, Tuscaloosa, Department of Aerospace Engineering & Mechanics
3043 H.M. Comer. 245 7th Avenue
e-mail address: John.Baker@eng.ua.edu*

An Adversarial Swarm model consists of two swarms that are interacting with each other in a competing manner. In the present study, an agent-based Adversarial swarm model is developed comprising of two competing swarms, the Attackers and the Defenders, respectively. The Defender's aim is to protect a point of interest in unbounded 2D Euclidean space referred to as the Goal. In contrast, the Attacker's main task is to intercept the Goal while continually trying to evade the Defenders, which gets attracted to it when they are in a certain vicinity of the Goal termed as the sphere of influence, essentially a circular perimeter. The interaction of the two swarms was studied from a Dynamical systems perspective by changing the number of Agents making up each respective swarm. A total of 22 cases were studied for an ascending number of Attackers and descending number of Defender agents, starting with a population of five Attackers and hundred Defenders and ending with hundred Attackers agents and five Defenders agents. A Monte Carlo analysis is also conducted for randomized initial conditions for each run, respectively. The simulations were strongly investigated for the presence of chaos by evaluating the Largest Lyapunov Exponent (LLE), implementing phase space reconstruction. Transient chaos was observed for some initial cases. The source of chaos in the system was observed to be induced by the passively constrained motion of the Defender agents around the Goal. Multiple local equilibrium points existed for the Defenders in all the cases and some instances for the Attackers, indicating complex dynamics. LLEs for all the trials of the Monte Carlo analysis in all the cases revealed the presence of chaotic and non-chaotic solutions in each case, respectively, with the majority of the Defenders indicating chaotic behavior. Overall, the swarms exist in the 'Edge of chaos,' displaying the existence of complex dynamical behavior. The final system state (i.e, the outcome of the interaction between the swarms in a particular simulation) is studied for all the cases, which indicated the presence of binary final states in some. Finally, to evaluate the complexity of individual swarms, Multiscale Entropy is employed, which revealed a greater degree of randomness for the Defenders compared to Attackers due to the chaotic and constrained nature of its movement in the vicinity of the Goal which it is trying to protect from being breached by the Attackers.

Keywords: Competitive swarms, Adversarial swarms, Dynamical system, Agent-Based Modelling, Multiscale Entropy

PACS:

I. INTRODUCTION

Swarms, which are a collection of individual autonomous agents, are omnipresent in nature ranging from ant colonies [1], flocks of birds [2], schools of fishes [3], and human crowds[4]. Swarming in nature provides many advantages, such as ensuring better survival chances against predators [5], collective foraging, and hunting [6]. Swarming behavior in nature has evolved over many thousands of years to be optimally adapted and prepared for the prevailing conditions in the environment. Bioinspired swarm models have been an active area of research for the past couple of decades. Mimicking natural swarm behavior for engineering applications is inherently problematic as all-natural systems offer inherent flexibility and scalability. The phenomenon of swarming has been exploited in modern-day engineering applications ranging from UAVs[7], optimization algorithms[1], robots [8], and spacecrafts[9].

All swarms are essentially complex systems that are generally characterized by nonlinear dynamics; an accurate physics-based model is essential to have a holistic

understanding of the dynamics of swarming behavior. Historically physicists have modeled from an Eulerian (Macroscopic) approach and a Lagrangian (Individual, agent-based) modeling approach. In the former approach, the swarm behavior is generally analyzed based on collective attributes such a flock density. In the Lagrangian based approach, the swarm agents and their interactions with the environment are modeled based on simple physics-based rules. Complex emergent behavior is observed, which is as a result of simple interactions at the agent level. Craig Reynold's s [10] seminal paper introduced the idea of swarm modeling, which showed that three simple rules could achieve emergent swarming behavior, namely - attraction, collision, and velocity alignment. Reynolds [11] subsequently added further rules called 'steering behaviors' to diversify swarming behaviors to achieve specific objectives. Huth et al. [12] introduced a model to describe fishes' behavior schools and compared simulated motion produced from his model with real-world data. Vicsek et al. [13] proposed a discrete-time model on self-governed motion in a system of particles. In Vicsek's model, every autonomous agent modified its velocity by adding the

weighted mean of the difference in other agents' velocities. Vicsek's [13] computer simulations showed agents approaching the same velocity with time, i.e. the particles behaved like swarms having coordinated motion. Vicsek et al. [13] has been studied extensively, and several variations of it proposed, which included the addition of inertia, time-delay, and noise [14]; all of Vicsek's models are kinematic in nature. Viscido et al. [5] studied the effect of population size and the neighbors on the emergent properties, which includes polarity, edges, and distinct shapes.

All the swarm models discussed so far consider mostly periodic boundary conditions, which are generally inconsistent with nature as most natural swarms flock in free space without any explicit boundary constraints. D'Orsogna et al. [15,16] proposed a swarming model using a generalized Morse potential coupled with Rayleigh friction force to study the structure of rotating flocks in free space. Forces derived from the pairwise Morse potential are repulsive at short ranges while being attractive at long ranges simultaneously; thus, it entails both close range repulsive and long-range attractive forces, which are essential components of any swarm. The Morse potential [17] is an integral component of the current work and is discussed in detail at a later stage. Vecil et al. [18] performed a 3D numerical simulation based on Orsogna's [15] model which identified vital parameters that govern the nature of flocking behavior observed as such a rigid body rotation, clumps, milling, spheres, and dispersion. Cucker and Smale [19] introduced a simple dynamical system to tackle the consensus problem in a leaderless non-hierarchical swarm's constituent agents. The Cucker-Smale [19] type model has been studied extensively, and the model has been developed further by adding extensive attributes as the addition of repulsive force [20], addition to stochastic white noise [21], interparticle bonding force [22], and Rayleigh friction [23]. All the models mentioned above are dynamical in nature and consider unconstrained swarming in free space.

In nature, swarms often interact with other swarms; interactions can be symbiotic or adversarial, depending on the nature of the swarms involved. Examples of symbiotic swarms found in the animal kingdom include multispecies group [24] hunting, were in different groups of species team up (cooperation) with each for hunting groups of prey. Adversarial swarms focus on the current study, which is abundant natural environments, such as groups of prey engaging with groups of prey, both in aquatic and terrestrial environments for foraging purposes. Terrestrial examples of Adversarial swarms include groups of omnivorous Chimpanzees hunting groups of Red Colobus Monkeys [25], groups of predator Lions hunting herds of Zebras [26], etc., in the aquatic environment, a multispecies association of Dolphins with Seals and Dogfish for feeding schools of small Fish [27], groups of Killer Whales and tens of tons of Herring, where the former would force the later to dive up by almost 150 meters [28] to indulge in more effective foraging.

Many adversarial swarm-based models have been adopted over the years in which physicists have traditionally modeled the adversarial swarms' phenomenon as a predator-prey problem. These models have been explored by multiple research communities such as ecologists, physicists, statisticians, and mathematicians. The current literature reveals three main types of models -kinematic, lattice-based, and dynamical models. In addition to the computational models, few experimental studies have also been conducted in the recent past. In kinematic models, the interactions between agents are typically modeled as velocity terms. Angelani [29] investigated the collective predation in a simple agent-based model capable of reproducing animal movement patterns where the individual agents were modeled based on Vicsek's self-propelled [13] agents. Lin [30] used a self-propelled particle-based model to study the predation of bats on prey. In the lattice-based models, the computation domain is divided into uniform 2D grids or lattices, which has 'states' associated with them, e.g., empty or filled. Notable lattice-based models include Kamimura et al. [31], where group chase and escape in the lattice-based swarm were modeled, and the study concluded the formation of highly self-organized spatial structures. Wang et al. [32] extended the predator-prey problem by adding a third species and considered the effects of stochastic vision, concluding a direct relationship between the predator's vision and the prey's extinction rate. Other notable works on swarms to swarm interaction includes Gaertner et al. [33], where an agent-based model based on the MASON library [34] was used to model the engagement between two groups of UAVs in 3D space. Strickland [35] studied swarm engagement during live experiments with two swarms of UAVs based on different pursuit and evasion strategies.

Competitive swarm models based on the dynamical system are explicitly based on Newton's second law of motion which, can provide accurate insights into the highly complex emergent behavior arising between the interaction of two swarms. Zhdankin et al. [36] conducted a study on the dynamics of a swarming predator-prey model, where each group's swarming was based on long-and short-range forces, and a non-conservative force was used to model the interaction term between the swarms. The study concluded the presence of chaos, quasi-periodic, periodic behavior, and the existence of singularities. Kolon et al. [37] investigated the collision of two swarms made up of homogenous agents by considering the effect of delay in communication between various agents; the study demonstrated mutual swarm capturing during the interaction, ultimately leading to a 'milling' [15] state of motion.

Overall the current literature available in the public domain lacks the presence of an Agent-based dynamical Adversarial Swarm model with explicitly defined 'inter' and 'intra' swarm forces, which are based on widely-accepted physics-based potential functions that have been historically successful to model the behavior of a simple swarming system capable of producing highly emergent behavior. This

gap in the current literature is addressed by developing a physics-based dynamical adversarial homogenous swarm model with a very well-defined intra-swarm and inter-swarm forces. The model consists of two distinct interacting swarms: The Attackers and the Defenders, who have conflicting objectives in unbounded 2D Euclidean Space. The Defenders' role is to protect the Goal i, e a point of interest in 2D Euclidian space. In contrast, the Attackers' primary objective is to intercept the Goal while continually evading the defenders. The Defenders swarms try to protect the Goal by swarming around it and blocking any Attackers agent trying to reach the Goal. It is assumed that if an Attacker and Defender agents are very close to each other, or, in other words, if the distance between them is less than a predefined criterion, they are considered to collide with each other and are consequently arrested from participating in the simulation. As a result of the interaction, the arrested agents' count may not always be binary. The arrested agents become inactive for the remaining time of the simulation. The simulation is assumed to have a binary outcome or a final state, wherein either the Attacker or the Defenders emerge dominant. The Attacker swarm is considered dominant if an agent in the swarm can successfully intercept the Goal during the simulation. If there are no remaining agents in the Defender swarm at any point in the simulation, then the Attackers are considered dominant. If the Defenders can successfully defend the Goal before the end of the simulation or if no Attackers are left in the simulation, the Defenders are considered the dominant swarm. If at any time during a simulation, no agents are left in either of the swarms(i.e the agents compromise each other off in the engagement), the Defenders are considered to be dominant in the simulation as the Goal has been successfully protected from the predation of the Attacker swarm.

In the current study, the dynamical system-based simulation is carried out of the Adversarial Swarm Model. The simulation is carried out on a robustly developed computational platform in C++ to solve Newton's second law problem. The nonlinear time series data obtained from the simulation uses a multitude of tools that included time-series plots, attractor plots, and Largest Lyapunov Exponent (LLE). The system is strongly investigated for the presence of chaos. As a vital parameter of the system, the number of Attackers and the Defender agents making up each swarm is varied to study the simulation's final state. The Largest Lyapunov Exponent for each case is also evaluated to probe the presence of chaos. The interacting swarm's complexity is found out by evaluating the Multiscale Entropy of the nonlinear time series data.

This paper is organized as follows- section 2 discusses the numerical model and the computational method used for solving the governing equations. Section 3 has brief descriptions of the nonlinear time series analysis techniques used, followed by the results and discussion for all the numerical experiments conducted. The final section comprises the conclusion.

II. USE NUMERICAL MODEL AND PARAMETER DESCRIPTIONS

2.1 Mathematical formulation of the model:

A physics-based agent-based model is derived to study the dynamics of two interacting adversarial swarms: The Attacker Swarm and the Defender Swarm (hence, referred to as 'Attackers' and 'Defenders' respectively). The agents have conflicting objectives; the Defenders protect a point of interest in unbounded 2D Euclidean space by swarming around the Goal along a sphere of influence. In contrast, the Attackers' main task is to intercept the Goal while constantly trying to evade the Defenders, who are actively chasing the former in a perimeter around the Goal or a sphere of influence. The individual swarms in the swarm system are modeled based on a Lagrangian based approach having primarily two types of forces- 'inter' and 'intra' swarm forces; the inter-forces are used to model the interaction between the agents of the adversarial swarms, respectively. The intra-forces are used to model the forces between members of the same swarm. Each swarm can be generalized as a collection of N agents in 2-Dimensional space with position and velocity vectors. The governing equation describing the dynamics of the two interacting swarms- the Attackers and the Defenders are derived based on Newton's second law of motion and are given by the following equations:

$$\ddot{X}_{A_i} = \dot{V}_{A_i} = \frac{1}{m_{A_i}} \left(\sum_{\substack{A_j=1 \\ A_j \neq A_i}}^{N_A} -(\nabla \varphi_{A,ik}) + \sum_{A_j=1}^{N_D} -\vec{\nabla}(k_{rep} r_{ij}^{-1}) \right) \quad (1)$$

$$-\vec{\nabla}(-k_{obj} r_{iG}^2) + (\alpha_A - \beta_A |\vec{V}_{A_i}|^2) \vec{V}_{A_i} \quad (2)$$

$$\dot{X}_{A_i} = \vec{V}_{A_i}$$

$$\ddot{X}_{D_j} = \dot{V}_{D_j} = \frac{1}{m_{D_j}} \left(\sum_{\substack{D_l=1 \\ D_l \neq D_j}}^{N_D} -(\nabla \varphi_{D,jh}) + \sum_{D_l=1}^{N_A} -\vec{\nabla}(-k_{att} r_{ji}^{-1}) \right) \quad (3)$$

$$-\vec{\nabla}(\varphi_{jG}) + (\alpha_D - \beta_D |\vec{V}_{D_j}|^2) \vec{V}_{D_j} \quad (4)$$

$$\dot{X}_{D_j} = \vec{V}_{D_j}$$

Eqns. (1-4) are the principal equations for the Adversarial Swarm model that subject to given initial conditions $\vec{V}_{A_i}(t=0)$, $X_{A_i}(t=0)$, $\vec{V}_{D_j}(t=0)$, $X_{D_j}(t=0)$ of individual agents in the respective swarms are known.

The first terms in Eqns. (1) and (3) respectively are intra-swarm forces that are modeled based on the scaled Morse[37] potential. The gradient of this potential is used to obtain the intra-swarm Morse force; the following equation gives a generalized scaled Morse potential.

$$\varphi_{ij} = C \exp\left(-\frac{|r_{ik}|}{l}\right) - \exp\left(-\frac{|r_{ik}|}{l}\right) \quad (5)$$

In Eqn. (5), C defines the depth of the repulsive potential well, and l is a constant used to relate the ratio of the repulsive to attractive length scales. The forces obtained from the scaled Morse potential are responsible for the swarming of agents in the Attackers and Defenders. The typical intra-swarm Morse force scenario is typically $C > 1$ and $l > 1$, which means that the repulsive component only acts at close ranges. However, the attractive component works at long ranges only, thereby preventing the dispersion of agents making up a swarm, respectively. From D'Orsoga et al.[15], it is known that there is a criterion called H stability is necessary, under which if the number of particles increases, the Morse force guarantees that the bounding of the swarm as the number of particles increases. The H stability can be achieved by imposing the condition $Cl^2 > 1$, lest it might lead to 'catastrophic' behavior [16]. The Morse force constants in both the Attackers and Defenders are chosen by imposing the H stability criteria.

The second term in Eqns. (1) and (3) is an attractive and repulsive potential. The Defenders stop the Attackers from fulfilling their primary objective, that is, the interception of the Goal. The Defenders agents use an attractive force derived from the second term's attractive potential in Eqn. (3) to intercept the Attacker agents. The Attackers agents try continually to evade the Defender agents utilizing a repulsive force derived from the second term of Eqn. (1). The attractive and repulsive potential found in Eqns. (1) and (3) are derived from a generalized obtained from Espitia et al.[38]. This potential serves a dual purpose, as it can be used to derive attractive force and the repulsive force by merely changing its sign. The following equation can compactly express the attractive/repulsive potential.

$$\varphi_A = \pm k_{rep/att} r_{ij}^{-1} \quad (6)$$

Where the first term in Eqn. (6) is a positive constant term (with suffix 'rep') if a repulsive force is derived and negative (with suffix 'att') if an attractive force is derived. The Defender agents only get attracted to the Attackers' agents inside the sphere of influence, as depicted by the circle in Fig.1. It is a necessary step, which ensures that the Defenders do not veer off too far from the Goal, as the Defender's main aim is to protect the Goal from the Attackers. The following equation defines the attractive force between the Defender agents and the Attackers agents inside the sphere of influence:

$$\vec{F}_{DA,A} = -\nabla(-k_{att} r_{ij}^{-1}) \text{ if } r_{ij} \leq R_{th} \quad (7)$$

$$\vec{F}_{DA,A} = 0 \text{ if } r_{ij} > R_{th} \quad (8)$$

Where R_{th} is a threshold radius around the Goal. The attractive and repulsive forces are inversely proportional to

the competing agents' distance, ensuring that the attraction and repulsion are strongest between the closest agents. The attraction and the repulsion forces are cut off using local distance thresholds, beyond which they would essentially be constants equal to the attraction/repulsive force at the threshold distances. The threshold distances prevent these forces from getting too large during the very close interaction of Attacker and Defender agents, thereby warranting a tractable computation. The distance thresholds are assumed to be the same for both classes of agents to ensure fair competition.

The third term in equation (1) is an attractive potential [38], which is used to obtain an attractive goal force between the Attackers and the Goal. The attraction force derived from this potential is a linear force that increases as the distance between an Attacker agent and the Goal increases and vice versa.

The third term in equation (3) is also derived from a scaled Morse potential [37] (similar to the potential used for deriving the intra-swarm forces) is a force between the Defenders and the Goal, which has a repulsive as well as an attractive component. This force prevents the Defender agents from wandering too far off from the Goal. The following equation gives the scaled Morse potential between the Goal and a Defender agent

$$\varphi_{jG} = C_{DG} \exp\left(-\frac{|r_{jG}|}{l_{DG}}\right) - \exp(-|r_{jG}|) \quad (9)$$

Where r_{jG} is the distance between a Defender agent and the Goal. C_{DG} and l_{DG} are constants that can control the composition of the attractive and repulsive force between the Defenders and the Goal. As discussed in the preceding section, the H stability condition ($Cl^2 > 1$) is imposed to avoid a 'catastrophic' scenario[15,16].

The last terms in the Eqns. 1 and 4 is the self-propelling and frictional force term, which is based on Rayleigh's friction. The Rayleigh friction force is derived from the Rayleigh Dissipation function [39]. It is a nonlinear damping term with self-acceleration and friction mechanisms, which drive all the particles to an equilibrium speed of α/β [15,36,37]. The Rayleigh Friction force is a velocity-based force which is non-conservative and is given by:

$$\vec{F}_{A,SF,i} = (\alpha_A - \beta_A |\vec{V}_{A,i}|^2) \vec{V}_{A,i} \quad (10)$$

$$\vec{F}_{D,SF,i} = (\alpha_D - \beta_D |\vec{V}_{D,i}|^2) \vec{V}_{D,i} \quad (11)$$

A detailed derivation of the governing equation comprising 2D cartesian forces obtained the potential function used in equations (1) and (2) can be found in the Appendix.

2.2 Initial Conditions, Verification, Validation, Uncertainty Quantification, and Parameter Selection/description:

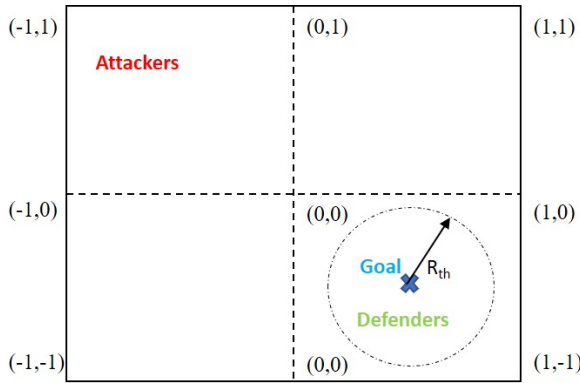


FIG. 1. (Color online) Illustration of the domain for simulation.

Eqs. (1)-(4) are numerically integrated using a customized 4th order Runge Kutta explicit solver [40] for Newton's Second law of motion. The agents are initialized within the square domain with distinct four quadrants, as shown in Fig 1. The Goal is located at the center of the fourth quadrant (0.5, -0.5); in this study, the Goal's location is considered fixed for all numerical experiments. The dashed circle around the Goal represents the sphere of influence found in Equations 7 and 8, is fixed at 0.508 for this study. The Defender positions are initialized randomly inside the sphere of influence, in the fourth quadrant, using a low discrepancy Sobol's sequence[41], the velocities are randomly chosen between ± 0.1 . The Attackers are also randomly generated inside the second quadrant using the same technique, and the velocities were also randomly selected between ± 0.1 . Low discrepancy Sobol's sequence is chosen to ensure minimal overlap between the initial position vector of agents making up their respective swarms.

The Runge Kutta solver is first verified by testing it against a trivial mass damper system. The validation of the custom solver developed for this problem is achieved by numerically evaluating the order of accuracy. In time, a comprehensive grid independence study is carried to evaluate the optimum timestep for solving the underlying governing equations for each agent, respectively, which is depicted in the subsequent section. A relative error threshold of 1% was considered in the position vectors for both the agents to perform the grid independence analysis in time.

Table 1: Various Key Parameters used in the numerical model

Constants	Values	Description
C_A	1.32	Depth of the potential well for pairwise scaled Morse potential for Attackers.
l_A	1.50	The ratio of the repulsive to attractive length scales of Attacker agents.
C_D	1.38	Depth of the potential well for pairwise scaled Morse potential for Defenders.

l_D	2.00	The ratio of the repulsive to attractive length scales of Defender agents
k_{rep}	0.054	Constant for pairwise inter-swarm repulsive potential between Attackers and Defenders.
k_{att}	2.82	Constant for pairwise inter-swarm attraction potential between Defenders and Attackers.
k_{obj}	10	Constant for pairwise inter-swarm Goal potential between Attackers and the Goal.
C_{DG}	10.03	The ratio of attraction and repulsive potential strength for scaled Morse potential between a Defender agent and the Goal.
l_{DG}	0.5	The ratio of the length scale of attraction and repulsion pair for scaled Morse potential between a Defender agent and the Goal.
α_A	1	Constant of the self-propulsion force for Attackers.
β_A	1	Coefficient of the Rayleigh friction force for Attackers.
α_D	1	Coefficient of the self-propulsion force for Defenders.
β_D	1	Coefficient of the Rayleigh friction force for Defenders.
R_{th}	0.508	Influence radius for Defenders.
m_A	1	Mass of Attacker agents.
m_D	1	Mass of Defender agents
Goal breach criteria	1E-4	Threshold distance between Attacker agents and the Goal for considering the Goal to be breached.
Agent compromise criteria	1E-4	Threshold distance between individual Attacker agents and Defender agents to be considered collided (hence dead).
Repulsive Force Local Cutoff for Attacker	0.05	The minimum distance beyond which the repulsive force between an Attacker and a Defender agent is treated as constant.
Attraction Force Local Cutoff for Defenders	0.05	The minimum distance beyond which the attractive force between a Defender and an Attacker agent is treated as constant.

The various constants' optimal values were obtained using a combination of trial and error, educated guess, and visual inspection (rendering of the simulation) over multiple random and non-random numerical experiments. Table 1 describes the model constants and values (Note: Suffix A denotes Attackers and suffix D represents Defenders). If the distance between two or more different agents is equal or less than the 'Agent compromise criteria', they are considered to have collided and are hence arrested from the simulation. The arrested agents become inactive for the remainder of the simulation. If the distance between any Attacker agent and the Goal is less than the 'Goal breach criteria', the Goal is considered breached. As stated in the introductory section, if any Attacker agent can successfully intercept the Goal, Attackers dominate the simulation. If the Defenders are able to defend the Goal before the end of the simulation or if no Attackers are left in the simulation, the Defender is considered the dominant swarm. If no Attacker or Defender agents are left at any point in the simulation, in that case, the Defenders are considered dominant as the Goal has been successfully protected from the Attacker's predation. The various threshold distances discussed so far can be found in Table 1.

III. RESULTS AND DISCUSSION:

All the simulations were carried out by developing custom software written in C++ and Python, which were run on the University of Alabama High-Performance Computing Network and a Desktop Computer having Intel® Core™ i7-9700 Processor, 64 GB RAM, and 1.25 TB of storage space. The simulations were carried out for different populations of Attackers and Defenders to study the dynamics and the outcome (final state) of the interacting adversarial swarms. The interaction between the two adversarial swarms was analyzed with respect to an ascending ratio of the number of Attackers to the number of Defenders. The maximum number of Attackers and Defenders agents in this study was limited by the computational resources available, which was capped at a maximum of 100 for each case. In the initial simulation, the number of attackers was 5; the number of Defenders chosen was 100 (case #1); for every subsequent case excepting case#2, the Attackers were increased by 5, and the Defenders reduced by 5; which was continued until there were 100 Attackers and 5 Defenders left.

Table 2: Case Matrix

Case	NA	ND	NA/ND	Runs	Timestep	Max Simulation Time
1	5	100	0.05	1000	5.00E-05	100
2	7	97	0.07	1000	2.50E-05	100
3	10	95	0.10	1000	2.50E-05	100
4	15	90	0.16	1000	2.50E-05	100
5	20	85	0.23	1000	2.50E-05	100
6	25	80	0.31	1000	2.50E-05	100
7	30	75	0.4	1000	2.50E-05	100
8	35	70	0.5	1000	2.50E-05	100
9	40	65	0.61	1000	2.50E-05	100
10	45	60	0.75	1000	2.50E-05	100
11	50	55	0.90	1000	2.50E-05	100
12	50	50	1	1000	2.50E-05	100
13	55	50	1.1	1000	2.50E-05	100
14	60	45	1.33	1000	2.50E-05	100
15	65	40	1.62	1000	2.50E-05	100
16	70	35	2	1000	2.50E-05	100
17	75	30	2.5	1000	1.00E-05	100
18	80	25	3.2	1000	5.00E-06	100
19	85	20	4.25	1000	5.00E-06	100
20	90	15	6	1000	5.00E-06	100
21	95	10	9.5	1000	5.00E-06	100
22	100	5	20	1000	2.00E-06	100

A total of 22 cases were studied in total, as shown in Table 2. All simulations had random initial conditions for position and velocity; a Monte Carlo study was carried out to

understand each case's outcome holistically. Every case was run for 1000 times, determined by the cumulative average of each run's total time. The cumulative average had a maximum change of 0.2% at the end of 1000 runs for each case, respectively. The amount of computational resources available also limited the total number of runs for each case, respectively.

The simulations were studied from a swarm to a swarm interaction perspective. The center of mass time-series of the swarm was found out averaging the x and the y coordinates of the position vectors with respect to the total number of active agents at every timestep. The center of the momentum of the swarms was found out by averaging the x and the y components of the velocity vector with respect to the total number of active agents at every timestep. In the preceding calculations, the individual agents' mass making up the respective swarms is considered unity. The center of mass and the center of momentum data were used to perform a detailed study of the underlying dynamics.

Largest Lyapunov Exponents (LLEs) of the center of mass time-series for both agents were obtained using Wolf's algorithm [42] by implementing phase space reconstruction by evaluating the minimum embedding dimension and time lag from Chen et al. [43]. Lyapunov exponent is a useful tool for determining the presence of chaos. Lyapunov exponents were found out for every trial run in each case, respectively. The following equation gives the Largest Lyapunov Exponent (LLE):

$$\Lambda_1 = \frac{1}{M_{LE} t_{evol}} \sum_{k=0}^M \ln \frac{L_{evol}^{(i)}}{L_o^{(i)}} \quad (12)$$

The Euclidean distance between the initial point and its nearest neighbor at $t = 0$ is given by L_o which evolves into L_{evol} after $t = t_{evol}$ and M_{LE} is the minimum embedding dimension of the reconstructed phase space.

The center of mass time series obtained for both the swarms was also analyzed from a multiscale entropy (MSE) perspective [44], which was first introduced by Costa et al. [45] as a qualitative measure for complexity. MSE can be used to determine whether a time series arises from a highly stochastic or a highly deterministic process, or, in other terms, it indicates the orderliness of a system. Multiscale Entropy is a very useful tool for evaluating the determinism or randomness in a time-series. The Multiscale Entropy for entirely random time series should be the highest and the lowest for the most deterministic time-series. It also measures the structural complexity in a physical system comprising of very high degrees of freedom. The Multivariate Multiscale Entropy (MSampEn) introduced by Ahmed [44] et al. is used in this study. The MSampEn algorithm proposed by Ahmed [44] uses a separate embedding dimension and time lag for a multivariate time series taken as input and is given by the following equation.

$$M_{SE}(M, \tau, r, N) = -\ln \left[\frac{B^{m+1}(r)}{B^m(r)} \right] \quad (13)$$

ADVERSARIAL SWARMS AS DYNAMICAL SYSTEMS

M is the embedding vector, τ is the time lag vector, r is the tolerance level, N is the number of data points in the time-series, $B_i^m(r)$ is the frequency of occurrence and $B_i^{m+1}(r)$ is the multivariate frequency of occurrence. MSampEn is used to find the Multiscale Entropy of the 2D center of mass time-series obtained from the Attackers and Defenders swarm, respectively, where the embedding dimension and the time lags for each dimension were determined by a computer program developed by Chen[43].

In the subsequent subsections, the simulations are analyzed with respect to the increasing NA/NA ratio, as presented in Table 2. Each case is analyzed from a dynamical systems point of view and is strongly investigated for chaos. The final state of the simulation is also explored in each case, respectively. In the last sub-section, Multiscale Entropy is used to evaluate the complexity of the respective swarms.

3.1: Analysis of dynamical behavior: Timeseries, phase space, and attractor visualization plots.

In this subsection, the dynamical behavior for all the cases are studied, as depicted from the cases presented in Table 2, is described. Starting with the first case (case 1) in Table 2, it is observed that the number of Defenders greatly outnumbers the number of Attacker agents. Case 1 is trivial, as the simulation outcome can be easily guessed. Fig.1 reveals the entire simulation; it is observed that 4 among the 5 Attacker Agents are killed relatively early in the simulation. It is seen that one Attacker agent and 96 Defenders agents are left until the end of the simulation. The survival of one Attacker agent until the end may seem to be a bit counterintuitive; the behavior observed can be explained due to the buildup of excessive repulsive force on the remaining Attacker agent from the 96 surviving Defender agents, as all agents in this simulation are globally coupled(i.e every Attacker agent interacts with every Defender agent). The Defenders are considered dominant as they successfully protected the Goal until the end of total simulation time. The outcome is also common sense as the Defenders greatly outnumbered the Attackers.

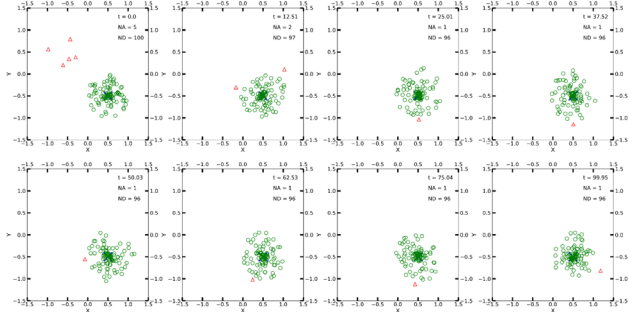


FIG 2: (Color Online) Snapshot of simulation for Case#1. Note: triangles and circles indicate Attacker and Defender agents, respectively.

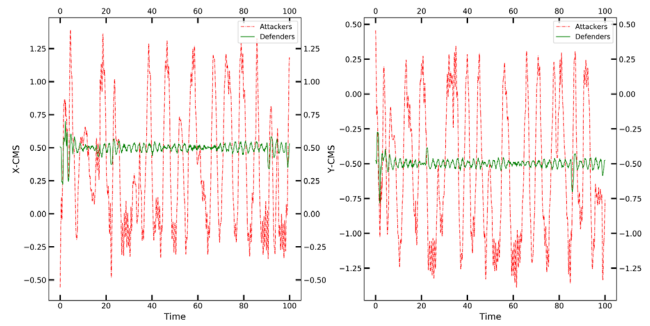


FIG 3: (Color Online) Center of mass time-series plots for Case#1

From the time-series plots in Figure 3, the agents' behavior is highly transient with periodic and non-periodic changes in amplitude; the rapid changes in amplitude of the center indicate close interaction between Attacker and Defender agents resulting in agent compromises on either end. After the compromise of agent or agents in each swarm, the CMS is calculated only among the active agents in the next timestep, causing the center of mass to shift rapidly.

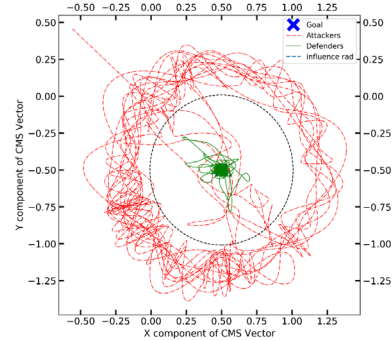


FIG 4: (Color Online) Center of mass of the Adversarial swarms in case#1 visualized in 2D space.

The center of mass for case#1 for both the agents of the Adversarial system is visualized in 2D space is found in Fig. 3, reveals the existence of “transient chaos”, which is defined as a situation where the trajectories leave the chaotic regime after a certain amount of time has passed resulting in the formation of a quasi-periodic pattern of motion[46]. Figs 3 and 4 show that the agent movements look chaotic initially and then abruptly switches to a quasi-periodic oscillation, which lasts for the remainder of the simulation. The initial chaotic trajectory can be attributed to the engagement between the Attacker and the Defender agents, resulting in most of the Attacker agents' death, which can be observed from Fig.3. As most of the Attacker agents are compromised in action, the quasi-periodic motion of the center of the Attacker swarm is along around the Goal, suggesting the few remaining Attacker agents are rotating in a quasi-periodic orbit around the Goal. The Defenders' time history indicates (Fig. 3) similar behavior with a lesser change in amplitude than the Attacker swarm. The Defender swarm is tightly packed due to many agents compared to the Attacker, so the swarm center's change is considerably less than its competitor. Overall, the Defender agents slightly translate towards the

Attacker when they are first approached by the latter inside the sphere of influence. Later, it is observed that the Attackers leave the sphere of influence and reenter the perimeter; Defender agents closest to the Attackers inside the sphere of influence. This process eventually leads to a quasi-periodic motion of the Defender agents around the Goal as most of the Attacker agents are killed in action. In the end, however, as visualized in Fig.4, it is observed that the last two remaining Attacker agent moves quasi-periodically outside the sphere of influence leading to their existence until the end of the simulation. To quantize the presence of chaos, the Largest Lyapunov Exponent (LLE) is computed for the center of mass time series for both the agents using Wolf's algorithm[42] by performing phase space reconstruction. The phase space is reconstructed using the x-component of the center of mass time series to evaluate its embedding dimension by evaluating the fraction of false nearest neighbors and estimating the time-delayed mutual information time-series [43]. The LLE for both the agents converged at 0.022 and 0.024, respectively, thus proving the existence of chaos.

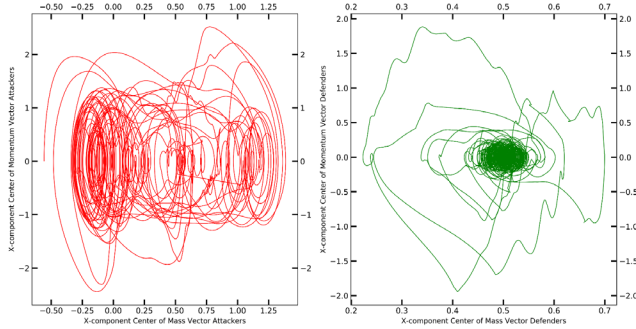


FIG 5: (Color Online) Attractor visualization for the center of mass for each swarm respectively in Case#1

From Fig. 5, it can be observed that for the Attackers, there exists more than one dynamical attractor leading to the establishment of multiple local equilibrium points for the Attacker swarm before it settles down to a quasi-periodic orbit around the Goal. This behavior can be attributed to the Attackers and Defenders' engagement, resulting in the compromise of agents killed in action. As the compromise of most of the Attacker agents takes place quickly in the initial part of the simulation, the local equilibrium points of the Attacker agents also change rapidly; in the latter half of the simulation, however, as only one Attacker agent is left, it is almost locked in a quasi-periodic orbit around the Goal. In the Defenders' case, however, 3 local equilibrium points are observed, among which the central point is much more pronounced than the others. The outer points observed from the left plot of Fig.5 result from initial interaction between the Attacker and the Defender swarms, where some of the Defenders initially translate towards the attacker swarm due to strong attraction. The Defenders eventually traverse out of the sphere of influence and return to the sphere of influence as they lose their attractive force once they venture out of the

sphere of influence. The center's local equilibrium point is the latter half of the simulation when only one Attacker agent is left. Most of the Defender agents rotate quasi-periodically around the Goal with the Attacker agents' occasional attraction as it crosses the sphere of influence. The presence of multiple local equilibria for both class of agents suggests the presence of many interdependent thresholds which can cause a rapid shift of the dynamical attractors causing rapid and drastic changes in the system, which in the present study can be attributed to the compromise of multiple agents as the two interacting swarms that are globally coupled intrinsically (within the same class of agents) and extrinsically (between the members of the two competing swarms). Such interdependent thresholds are often observed in the earth's climatic system, essentially a complex system, wherein abrupt changes are persistent and unpredictable [49]. Thus, the current competing swarm system under discussion can be regarded as a complex system. Similar dynamical behavior is obtained in cases 2 and 3 and with multiple dynamical attractors; also, in these cases, the Defenders emerge as the dominant swarm.

Starting from case#4 (NA=15, ND=90) onwards, a decrease in the number of local equilibrium points for the Attackers and an increase in the same for the Defenders is observed, which is mainly due to a relative decrease in the total run time of the simulation, which means all the Defenders were able to intercept the Attacker agents in early on the simulation. There is a decrease in the simulation's average total run time for all the trials (as presented in Table 2), discussed in detail in this paper's succeeding subsection. This trend is observed in the overall dynamical behavior and continues until case 8(NA=35, ND=70). The attractor visualization plot for case#8 can be found in Fig.6.

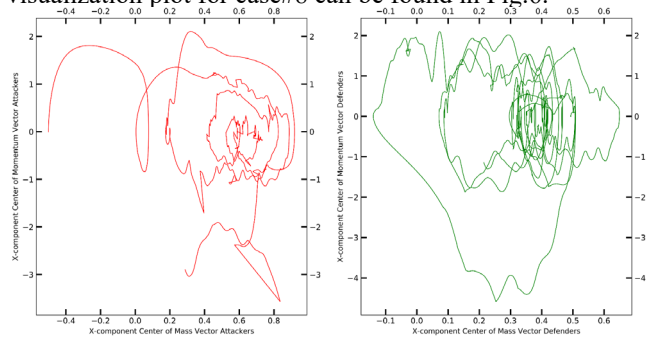


FIG 6: (Color Online) Attractor visualization for the center of mass for each swarm respectively in Case#8

From case #9 onwards, as the number of Attackers considerably increases and vice versa. The Attackers' equilibrium points appear centrally around the Goal. For the Defender agents, however, multiple equilibrium points are still observed. This is due to the high degree of interaction of the Attackers with the Defenders, which causes the system to arrive at the final state much faster than the initial cases, as outlined in Table 2. The Attacker agent's strong interaction is attributed to the decrease of the globally

ADVERSARIAL SWARMS AS DYNAMICAL SYSTEMS

coupled repulsive force between an Attacker agent with all the Defender swarm agents, making them more prone to interact with the Defender agents.

In case 12, the interacting Defender and Attacker swarms are made up of an equal number of agents (50 each). Fig.7 reveals the snapshot of the entire simulations taken at 8 equated timestamps throughout the simulation. Each swarm is made up of 50 agents; respectively, it can be observed that the Attackers and the Defender swarm interact actively from the onset of the simulation.

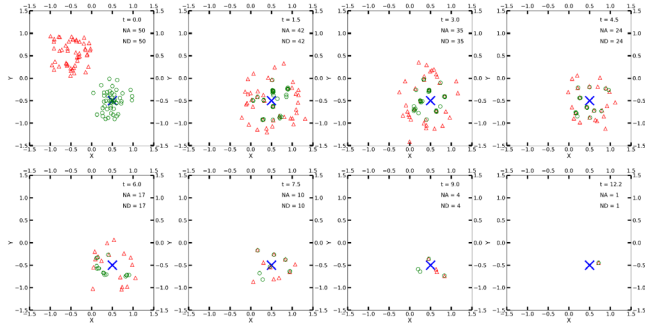


FIG. 7:(Color Online) Snapshot of simulation for Case#12. Note: triangles and circles indicate Attacker and Defender agents, respectively.

During the engagement, there is a substantial loss of agents from early on. Fig. 7 also reveals that the loss of agents happens at almost the same proportion, indicating that agents are engaging on a one-on-one basis with its spatially closest adversarial counterpart before the collision, ultimately resulting in the pair's loss. Towards the end of the simulation, it is observed from Fig. 7 that two adversarial agents are left (an Attacker and a Defender) that moves around the Goal in a quasi-periodic orbit. In contrast, the Attacker tries to continually reach the Goal with the Defender agent trying to prevent. The engagement lasts until the Defender agent can intercept the Attacker agent, resulting in both the agents' death as observed from the last subplot of Fig.7. The Defenders dominate this simulation's final state as their ultimate objective is to protect the Goal from the Attackers. This case is also run for 1000 times like the other cases. A detailed study for all the other cases reveals that the agents' interaction may not always be binary (one-on-one) in nature. Some of the cases during the Monte Carlo analysis reveal multiple agent compromise (i, e more than 2) during intense interaction during some trials.

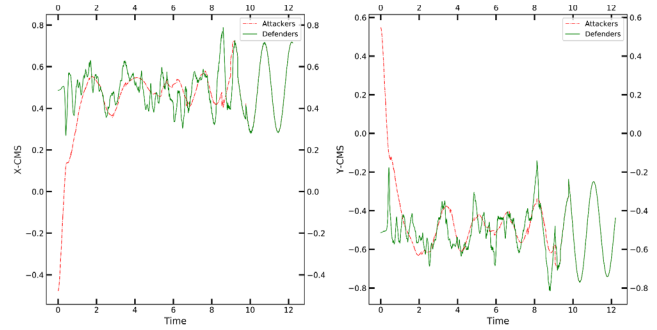


FIG. 8:(Color Online) Center of mass time-series plots for Case#11

The center of mass time histories of both the swarms is plotted in Fig.8, revealing the presence of highly transient behavior with somewhat irregular-shaped nonsmoothed peaks and troughs. The irregularity in the peaks and troughs is due to the loss of agents in rapid progression due to close and rapid engagements. The plots reveal the existence of transient chaos like Case#1. The LLE calculated for this case is 0.003 and 0.011 for the Attacker and the Defender swarm, respectively. Near the end of the simulation, it is observed that both the agents' trajectories converge to a quasi-periodic orbit around the Goal. This behavior can also be observed from the phase space plots in Fig.9. Initially, strong interaction between the Attacker and the Defender agents results in rapid loss of agents, causing irregularly shaped orbits around the Goal. The center of mass shifts rapidly due to the loss of many compromised agents which are not included in its calculation.

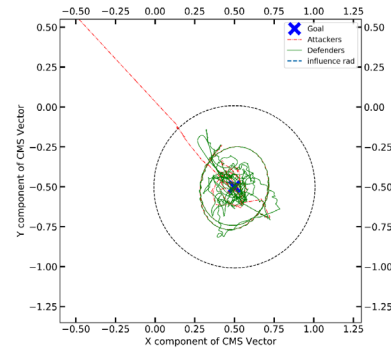


FIG. 8. (Color online) The simulation described in Case#12 is visualized in 2D space.

ADVERSARIAL SWARMS AS DYNAMICAL SYSTEMS

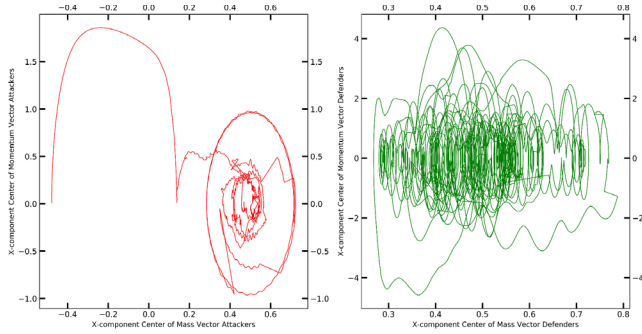


FIG. 10:(Color Online) Center of swarm attractor visualization for Case#11

Fig. 10 reveals a single equilibrium point for the Attacker swarm around the Goal and multiple local equilibrium points for the Defender swarm. This pattern is caused by the Goal being surrounded by the Attacker agents while constantly rotating around it. The Defender swarm center constantly shifts towards the closest Attacker agents, leading to the formation of multiple local equilibrium points.

A similar pattern of dynamical behavior continues with the reduction of Defender agents and the increase of Attacker agents beyond case#12. The rotation of the Attacker agents around the Goal is also significantly reduced as the final simulation state is attained faster. The attractor visualization plot for case 18 (NA=85, ND=15) can be visualized in Fig. 11, which reveals the shrinkage of the basin of attraction for the Attackers.

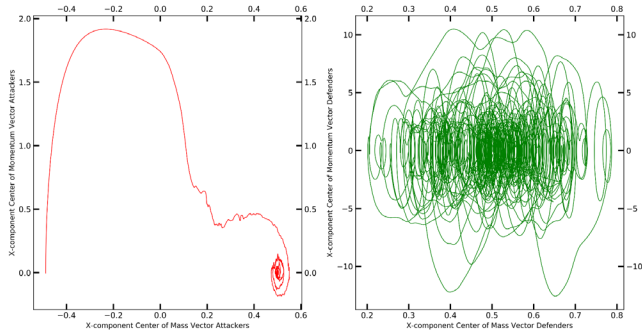


FIG. 11:(Color Online) Center of swarm attractor visualization for Case#18 (NA=85, ND=15).

Case#22 is the last case, essentially the converse of case#1; the Attacker agents vastly outnumber the Defenders. The final state of this case is trivial; it can be observed that all the Defenders agents are compromised quite early in the simulation. This behavior is expected as the Attacker agents experience relatively less amount of repulsive force from 5 Defender agents because of which the Attackers initially approach the Defenders with an almost linear trajectory followed by a minor rotation around the group as observed from the phase space plot in Fig.13. The Defender swarm undergoes erratic motion around the Goal because it tries to engage with the Attacker agents closest to the Goal, causing the center of mass to change rapidly. The close engagement with an outnumbered Defender swarm caused the rapid compromise of agents on both sides as the Defender agents are easily able to intercept Attacker agents, which are in a

very close formation around the Goal inside the sphere of influence. The time histories of the center of mass in Fig.12 reveal steep peaks and troughs for the Defenders, which is caused due to the rapid compromise of agents in the outnumbered Defender swarm, causing the center of swam to shift rapidly. The Attacker swarms comprising a much greater number of agents do not show the presence of steep peaks or troughs as the center of the swarm does not appreciably change due to their close formation on the Goal and the death of relatively few agents compared to the entire population of agents.

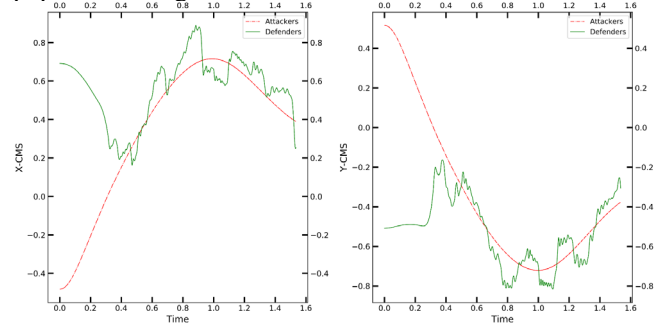


FIG. 12:(Color Online) Center of mass time-series plots for Case#21

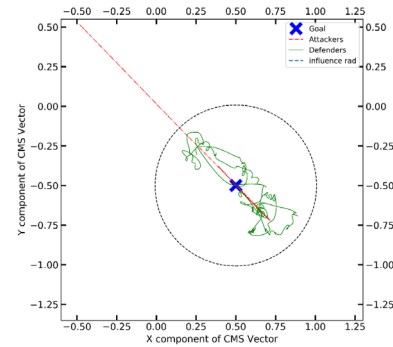


FIG. 13:(Color Online) The simulation described in Case#21 is visualized in 2D space.

Fig. 14 reveals a faint attractor for the Attackers and several local attractors for the Defender swarm. This is consistent with the behavior observed in Fig.11 (case 18). The creation of local dynamical attractors can be credited to the extreme erratic motion of the center of the Defender swarm as they engage with the nearest Attacker agents while at the same time being passively constrained around Goal due to the presence of Morse force between the Attackers and the Goal.

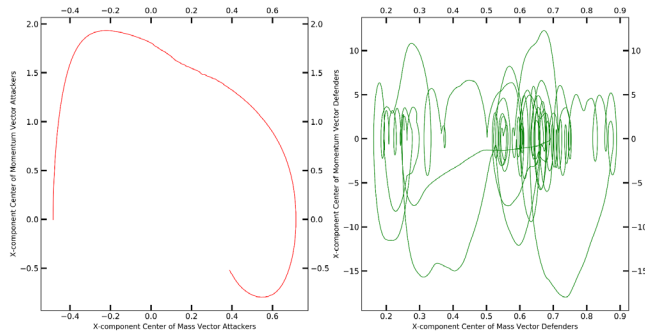


FIG. 14:(Color Online) Center of swarm attractor visualization for Case#21

3.2: Final Simulation State

The final state of the system, which is the outcome of the two swarms’ interaction, is of immense importance as it determines which class of agent dominates the simulation in the end. The dominant swarm is classified by a flag introduced in the simulation, defined as +1 if the Defenders emerged dominant and -1 for the Attackers. As discussed in this paper’s introductory sections, the Defenders emerges dominant if the Goal was protected from the Attackers until the end of the maximum total time allotted for the simulation, or if the Attacker swarm is compromised before the total time. On the other hand, the Attackers emerges dominant due to the compromise of the Defender swarm or the Goal’s breach. The final state was found out by defining a Dominant Simulation State metric is calculated for each case presented in Table 2. The simulation Dominant Simulation State metric is defined as the simple product of flag, the average time of run for all the 1000 trials in the Monte Carlo analysis, and the number of times a particular swarm emerged dominant(wins). The Dominant Simulation State metric is plotted against the agents’ ratio on a semi-log scale (x-axis only), which can be found in Fig 15. The random initial condition and the high degree of freedom of the system cause the nature of the swarm agents’ interaction to be stochastic in nature, making the ending of each simulation unique.

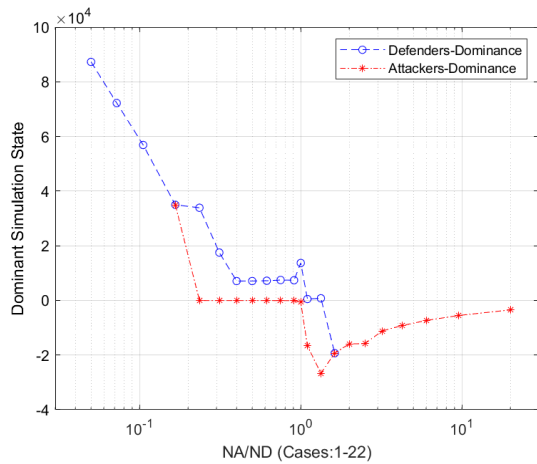


FIG. 15:(Color Online) Plot of Simulation Winner Outcome versus Population of Attacker and Defenders

(NA/ND). The x-axis is plotted in log scale for the clarity of the figure.

Initially, the Defender swarm exclusively emerges dominant for cases#1-4, which indicates that the Defender swarm can protect the Goal by intercepting Attacker agents or by preventing them from reaching the Goal. It can be observed from Fig.16 that most of the Defender dominance is due to the Goal end protection, which means the Defenders were successfully able to protect the Goal until the end of maximum permissible simulation time. This behavior is expected due to the excessive repulsive force on relatively few Attacker agents compared to the more significant number of Defenders. In relatively few cases, the Defender swarm could successfully intercept and compromise the Attacker swarm as its movement is highly constrained around the Goal. It can be observed that starting from case#5 through case#12, and there exist binary final states of the system i.e either with of the swarms assert dominance. It can also be observed that the Defenders emerge as the dominant party in the majority of the simulations. The dominance was profoundly due to the compromise of the Attacker swarm due to the considerable interaction. In relatively few cases, the Defenders emerged victorious by standing ground until the end. This trend continues until case#12. Much of the Attacker swarm’s marginal winning until case#12 (NA/ND=1) is caused by the breach of the Goal, while the minority of the wins is due to the total compromise of the Defender swarm. Beyond case#12, as the number of agents in the Attacker swarm increases considerably, the Attacker swarm’s dominance increases mostly by compromising the Defender swarm compared to the Goal’s breach, which continues until the remaining cases. The Defender swarm can only exert marginal dominance from case#12 onward until case#14 by preventing the breach of the Goal. Overall, it is concluded that due to the stochastic nature of the interactions, the ratio of the agent population making up the respective swarms is a crucial factor in determining most of the final state of the simulation. However, the existence of several unexpected marginal cases of dominance was also confirmed, as evident in Fig.15.

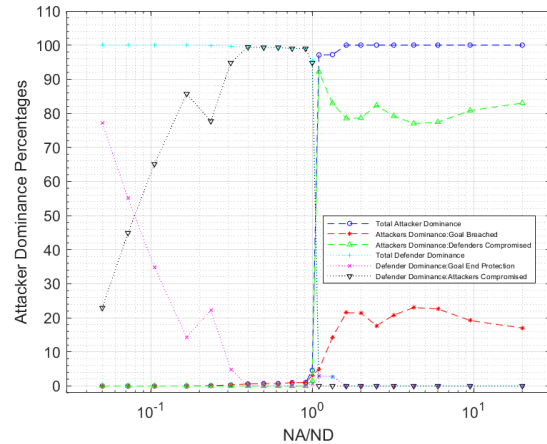


FIG. 16:(Color Online) Plot of Simulation Winner Outcome versus Population of Attacker and Defenders (NA/ND). The x-axis is plotted in log scale for clarity

3.3: Largest Lyapunov exponent for all the cases presented in Table 2.

The Largest Lyapunov Exponent (LLE) for the center of mass time series is calculated for the Attacker and Defender agents using Wolf’s algorithm[42] as outlined in Eqn. (12) for all the 1000 trails as outlined in Table 2.

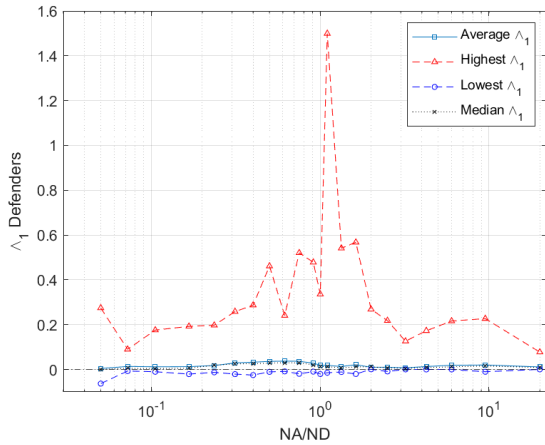


FIG. 17:(Color Online) Largest Lyapunov Exponent (LLE) of the center of mass time series of Defender swarm versus the Ratio of the Number of agents initially making up the Attacker and Defender swarms respectively, for 1000 trials.

The average, median, maximum and minimum LLEs found out from the trials are plotted in Fig. 17 and 18 for the Attacker and Defender swarm, respectively. It is observed that average LLE hovers in and out of zero for both the agents, indicating that the system is on the Edge of Chaos [47-49].

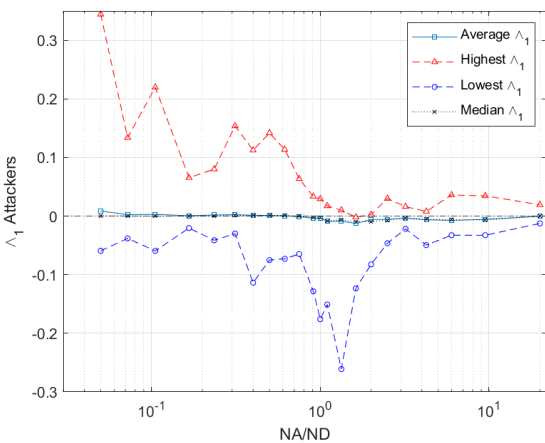


FIG. 18:(Color Online) Largest Lyapunov Exponent (LLE) of the center of mass time series of Attacker swarm versus the Ratio of the Number of agents initially making up

the Attacker and the Defender swarm, respectively for 1000 trials.

In this region, a dynamical system crosses the boundary between a highly deterministic system and a chaotic one. It is believed that at the “Edge of chaos,” the complexity of a dynamical system increases and is believed to have the greatest computational capacity[49]. From Fig. 17 and 18, it appears that the average LLE for the Defenders is greater than zero for all the cases presented in Table 2 and the average LLE for the Attackers is less than zero beyond case 9. The minimum and the maximum LLE for all the cases are positive and negative, respectively, indicating the presence of chaotic and non-chaotic solutions. The interacting swarm system, in this case, can be concluded to be in the ‘Edge of Chaos,’ which causes a rapid change in the dynamics of the system. From Fig.15, it is evident that from case#5 through 7, even though the number of Defender agents is large compared to the number of agents in the Attackers, it is tempting to conclude that the outcome of such cases would be trivial (i,e the Defenders exert dominance). On the contrary, a marginal number of cases where the Attacker swarm can successfully breach the Goal. The system hovers at the ‘Edge of chaos,’ causing rapid change in the system’s underlying dynamics; thus, it may be concluded that some solutions appear to be chaotic, ultimately affecting the system’s final state.

Figs. 17 and 18 also reveal that the highest LLE reorder for the entire study occurs at case 13 (NA=55, ND=50) equal to 1.55. Cases 11 through 13 are interesting as the number of Attackers and Defender agents making up their respective swarms is equal or numerically very close to each other. A histogram is plotted for the LLEs calculate for both agents in case#12 is plotted in Fig 17. We see that both the swarm have a prominent central peak at -0.006 and 0.010 for the Attackers and Defenders, respectively, reaffirming both the swarms are zoning around the edge of chaos. The histogram further indicates that the majority of the Defender swarms for the trials in case#12 have a positive LLE. The highly chaotic behavior is due to the Defender swarm’s rapid engagement with the many Attacker agents in multiple directions. As a consequence of rapid engagement, multiple agents on either side are compromised. Most of the Attacker agents, on the other hand, have negative LLE as they mainly exhibit periodic or semi-periodic movement around the Goal while moving in and out of the sphere of influence, while interacting with the Defenders.

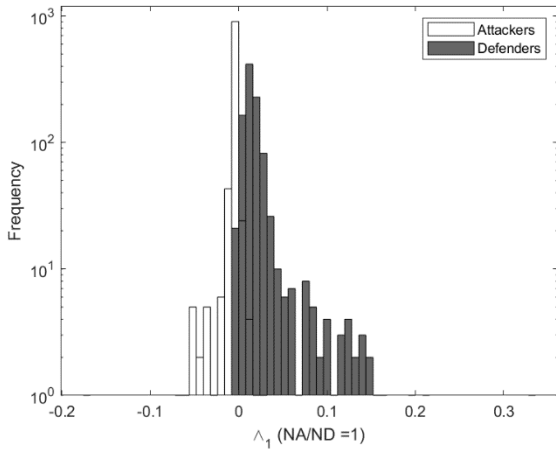


FIG. 19: Histogram of LLEs of the center of mass time series for case#12(NA=50, ND=50) for 1000 trials

3.4 Multiscale Entropy analysis

Multiscale Entropy is used to quantize the complexity of the Defender and the Attacker swarm, respectively. Multiscale Entropy is calculated for all the cases in Table 2 for time scales from 1 to 20, reveals it is monotonically increasing. A concise picture of the change in MSE for all the simulation cases studied in Table 2 is presented by plotting the ratio of the Multiscale Entropy calculated at scales 20 and 1 respectively, and can be found in Fig.20.

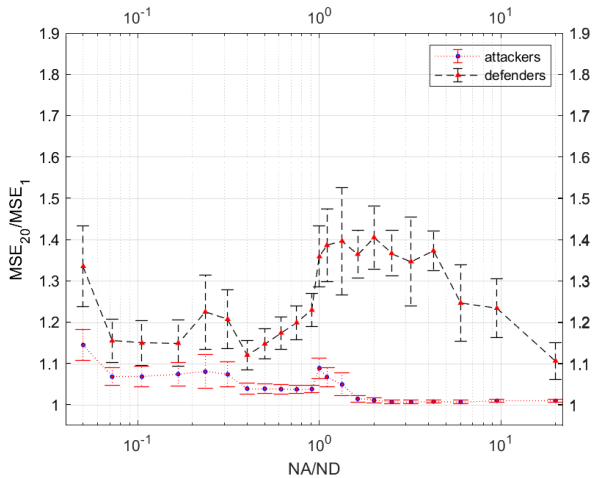


FIG. 20:(Color Online) Ratio of Multiscale Entropy calculated at scale 20 and scale for the center of mass time series for Attacker and Defender swarm respectively, for all the cases presented in Table 2. The error bars represent the sample standard deviation in each case.

The MSE of the Defender swarm is greater than the Attacker swarm for all time scale indicates that the Defenders are dynamically more complex than the Attackers. The ratio of the MSE for the Defenders for all the scale indicates monotonically increasing behavior. The Attackers also exhibit the same trend except until case 16, beyond which the ratio of the MSE is ~ 1.01 , indicating that

the MSE increase is not appreciable across scale 1 to 20. A detailed study of these cases reveals that the MSE does not show an appreciable increase when plotted from scales 1 through 20. Thus, overall, it can be concluded that the interacting swarm system exhibits the behavior of a complex system. This overall trend can be explained from a philosophical standpoint that a complex system is often defined as ‘more’ than just combining its constituents. A standalone system constituent cannot explain the complex emergent behavior observed by the system overall. In the present problem, the Attackers and Defenders swarm are made of simple agents that exhibit highly emergent behavior in swarming while interacting with each other in an adversarial manner. The MSE is also a measure of the ‘orderliness’ of a system; the MSE indicates that the Defender is less ordered as a system compared to the Attackers; this is expected because when the Defender swarm engages with the Attacker swarm, the Defenders are forced to be constrained in a relatively smaller perimeter defined by the influence radius used in the Attractive force between the Defender agents and the Goal, which is also evident from the attractor visualization plots presented in the previous sections. The Defenders’ constrained motion is dynamically more complex than the unconstrained motion of the Attackers in 2D Euclidian space. This phenomenon is backed by the dynamical behavior observed in Figs. 3 and 5, respectively.

It can also be concluded from Fig.20 that the Defenders have higher mean multiscale Entropies occur from case#11 through 16; these cases also have the most extensive variation as indicated by the error bars. On the other hand, the attackers exhibit relatively higher mean MSEs from 1 through 6 and then again from 12 through 14. Cases 11 through 14 exhibits overall the most dynamically complex behavior for both agents; the number of Agents in both the swarms are either equal or numerically very close. These cases also exhibit binary final states, as indicated in Fig.20, along with the maximum variation of the LLEs is observed from Fig.17 and 18. In the initial few cases (cases 1 through 5), the Attacker swarm exhibits relatively higher MSEs as the size of the Attacker is considerably smaller compared to the Defender swarm, thus causing greater randomness in the overall interaction when studied over 1000 trials. Beyond case #15, the Attacker swarm emerges as the dominant swarm in all trials because they heavily outnumber the Defender swarm. Fig. 20 reveals a drop in the randomness of the simulation. The Attacker swarm quickly exerts its dominance which is expected as the Defender phase plots contain erratic trajectories around the Goal as it is overwhelmed by a vast number of Attacker agent engaging from all sides, all these factors causes a drop in the MSE of the Attacker swarm along with its overall variation in all the trials; as for the Defenders complex dynamic also exists for all the cases which lead to a higher degree of random behavior causing the MSE to be relatively higher than the Attackers.

IV. CONCLUSION

The adversarial swarm model discussed in this paper comprises two types of agents: The Attackers and the Defenders, which are interacting in unconstrained 2D Euclidean space. The force terms present in Newton's second law-based governing equation can be broadly classified into two types: 'intra' and 'inter' respectively, responsible for swarming in the respective swarms and their interaction with their competing counterpart.

The Defender's main aim is to protect a point of interest in 2D space referred to as the 'Goal.' In contrast, the Attacker's main objective is to intercept the Goal while continually trying to engage with the Defenders. If the distance between a Defender agent and the Goal is less than or equal to the Goal breach criteria, then the Goal is assumed to be breached, and the Attackers are declared to be dominant in the simulation. If the distance between an Attacker agent and Defender agent is less than the Agent Compromise Criteria, the agents are considered to have collided and are hence arrested from the simulation. The Defenders are dominant if no Attackers are left in the simulation or if the Goal is not breached before the end of maximum permissible simulation time. The Attackers are considered the dominant swarm if the Goal has not been successfully breached or if the entire Defender swarm is compromised before the total simulation time.

A total of 22 simulation cases were studied with a decreasing number of Defender agents and an increasing number of Attacker agents, as presented in Table 2. A Monte Carlo analysis was done by running each case 1000 times to statistically study the final state of the simulation, LLE, and the MSE. Initial cases (#1-#4) revealed transient chaotic behavior with multiple local equilibrium points for both the parties. Multiple local equilibria existed for both the swarms from case#1-case#9, proving the existence of complex dynamics. Beyond case #10, the number of local equilibrium points reduces for the Attackers as it converges to a central equilibrium point. On the contrary, multiple equilibrium points existed for the Defender agents for all the remaining cases.

The Largest Lyapunov exponents were found out for the Attackers and Defenders from the center of mass time series for all the trials in each case, respectively, reveals the existence of chaotic and non-chaotic solutions. The mean LLE for the Defenders is greater than zero, indicating that most of the solutions are chaotic along with the presence of marginal non-chaotic ones. The chaotic behavior is due to the Defender's tight constrained motion around the Goal while at the same time engaging with the Attacker agents. The mean LLE for the Attackers is slightly less than zero for the majority of the cases. The average LLEs indicate that swarms are both on the 'Edge of chaos,' further strengthening the presence of complex dynamical behavior.

Finally, Multiscale Entropy (MSE) is evaluated for the center of mass time-series for both the swarm from scales 1

to 20. MSE, for both Attackers and Defenders, reveals the MSE increases monotonically from scale 1 to 20, which is consistent with the existence of complex dynamics. The MSE for the Defender is higher than the Attackers for all the cases, indicating that the Defenders have a higher degree of randomness than the Attackers, which can be linked to multiple local equilibrium points throughout all the cases.

In the current work, the simulations only consider the interaction between Attacker and Defender swarm. The simulations consider an ideal environment where the interactions occur; noise effects are not considered in the model. The work also assumes ideal and instantaneous inter and intra swarm communication and does not consider the effects of delay in communication. The position of the Goal is also assumed to be fixed for all the cases studied and the work does not assume a moving goal. The Attackers and Defenders are also globally coupled, which may not always be the case for autonomous agents. Delay in communication between the agents is not considered, which is often the real-world case due to various factors. All these limitations will serve as the basis of future works.

ACKNOWLEDGEMENTS

The authors would like to acknowledge the staff of the University of Alabama, High-Performance Computing Team for their continued support and cooperation.

APPENDIX

1. Detailed Derivation of the Governing Equation presented in Section 2

A detailed derivation of the Governing Equation is used in the paper is given here. To determine the forces acting upon each agent requires the specification of various potential functions. Following Kolon and Schwartz [37], it has been assumed that the scaled Morse potential may be used to define the interactions between agents of a given swarm. The scaled Morse potential is given as

$$\phi_j = C \exp\left(-\frac{|r_{ij}|}{l}\right) - \exp(-|r_{ij}|) \quad (14)$$

Where C defines the depth of the repulsive potential well and l is constant, that may be used to relate the ratio of the repulsive to attractive length scales. Recognizing that force is the negative gradient of the potential, i.e.

$$\vec{F} = -\vec{\nabla} \phi_j \quad (15)$$

As the scaled Morse potential is spherically symmetric, the component forces in a Cartesian coordinate system may be found using the following equations

$$F_{x,ij} = -\frac{\partial \phi_{ij}}{\partial x_{ij}} = -\frac{\partial \phi_{ij}}{\partial r_{ij}} \frac{\partial r_{ij}}{\partial x_{ij}} \quad (16)$$

$$= \left[-\frac{C}{l} C \exp\left(-\frac{|r_{ij}|}{l}\right) - \exp(-|r_{ij}|) \right] \frac{\partial r_{ij}}{\partial x_{ij}}$$

$$F_{y,ij} = -\frac{\partial \phi_{ij}}{\partial y_{ij}} = -\frac{\partial \phi_{ij}}{\partial r_{ij}} \frac{\partial r_{ij}}{\partial y_{ij}} \quad (17)$$

$$= \left[-\frac{C}{l} C \exp\left(-\frac{|r_{ij}|}{l}\right) - \exp(-|r_{ij}|) \right] \frac{\partial r_{ij}}{\partial y_{ij}}$$

To evaluate the derivative of the radius in 2D Cartesian coordinate, it is recalled that

$$r_{ij} = \sqrt{(x_i - x_j)^2 + (y_i - y_j)^2} \quad (18)$$

Taking the partial derivative of Eqn. (5) and substituting in Eqns. (3) and (4)

$$F_{x,ij,M} = \left[-\frac{C}{l} \exp\left(\frac{|r_{ij}|}{l}\right) + \exp(-|r_{ij}|) \right] \frac{(x_i - x_j)}{r_{ij}} \quad (19)$$

$$F_{y,ij,M} = \left[-\frac{C}{l} \exp\left(\frac{|r_{ij}|}{l}\right) + \exp(-|r_{ij}|) \right] \frac{(y_i - y_j)}{r_{ij}} \quad (20)$$

Eqns. (6) and (7) are the Cartesian component for the generic Morse force responsible for swarming in both the Attackers and the Defenders. Needless to say, unique constants are used for the Morse Force, as presented in Table 1.

Two Adversarial Swarms are considered in the current problem, which is made up of Defenders and Attackers. The Defenders are trying to prevent the Attackers from reaching a fixed target (the ‘Goal’) in the domain, whereas the Attackers’ task is to reach the Goal by avoiding the Defenders. To accomplish this, a Goal force and an attraction/repulsion force needs to be derived. The goal and attraction-repulsion forces are obtained by differentiating potentials functions obtained from Espitia[38]. The goal potential is defined as:

$$\phi_G = -k_{obj} r_{iG}^2 \quad (21)$$

Where the distance between the Goal and the individual agent is $r_{iG} = \sqrt{(x_i - x_G)^2 + (y_i - y_G)^2}$. Similarly, the 2D cartesian component of the Goal force is obtained by taking the gradient of the potential along each direction respectively and is given by the following equations:

$$F_{x,G} = [2k_{obj} r_{iG}] \frac{\partial r_{iG}}{\partial x_{iG}} = \frac{(x_i - x_G)}{r_{iG}} \quad (22)$$

$$F_{y,G} = \frac{(y_i - y_G)}{r_{iG}} \quad (23)$$

The goal force is positive as it is essentially an attractive force; the Attackers reach their target by using the goal force.

A generalized attractive or repulsion potential from Espitia[38] is defined as:

$$\vec{F}_{A/R} = -\vec{\nabla}(\pm k_{att/rep} r_{ij}^{-1}) \quad (24)$$

The 2 components can be derived as:

$$F_{x,A/G} = [\pm k_{obj} r_{ij}^{-2}] \left(\frac{x_i - x_j}{r_{ij}} \right) \quad (25)$$

$$F_{y,A/G} = [\pm k_{obj} r_{ij}^{-2}] \left(\frac{y_i - y_j}{r_{ij}} \right) \quad (26)$$

There are two distinct types of agents in the system the Attackers and the Defenders. Let the prefix A be assigned for the Attackers and the prefix D for the Defenders. N_A and N_D represent the number of Attackers, and Defenders, respectively. Newton’s Second Law for each agent of the Attackers and the Defender respectively can be written in terms of the 2D cartesian coordinate system as

$$\frac{\partial^2 x_{A_i}}{\partial t^2} = \frac{1}{m_{A_i}} \sum_{\substack{A_k=1 \\ A_k \neq A_i}}^{N_A} \left[-\frac{C_A}{l_A} e^{-\frac{r_{A_i A_k}}{l_A}} + e^{-r_{A_i A_k}} \right] \frac{(x_{A_i} - x_{A_k})}{r_{A_i A_k}} \quad (27)$$

$$+ \frac{1}{m_{A_i}} \sum_{A_j=1}^{N_D} -\nabla[-k_{rep} r_{A_i D_j}^{-2}] \frac{(x_{A_i} - x_{D_j})}{r_{A_i D_j}} +$$

$$\frac{1}{m_{A_i}} \sum_{D_k=1}^{N_D} -\nabla[-k_{obj} r_{A_i G}] \frac{(x_{A_i} - x_G)}{r_{A_i G}} + (\alpha_{A_i} - \beta_{A_i} |\vec{v}_{A_i}|^2) \vec{v}_{A_i}$$

$$\frac{\partial^2 y_{A_i}}{\partial t^2} = \frac{1}{m_{A_i}} \sum_{\substack{A_k=1 \\ A_k \neq A_i}}^{N_A} \left[-\frac{C_A}{l_A} e^{-\frac{r_{A_i A_k}}{l_A}} + e^{-r_{A_i A_k}} \right] \frac{(y_{A_i} - y_{A_k})}{r_{A_i A_k}} \quad (28)$$

$$+ \frac{1}{m_{A_i}} \sum_{A_j=1}^{N_D} -\nabla[-k_{rep} r_{A_i D_j}^{-2}] \frac{(y_{A_i} - y_{D_j})}{r_{A_i D_j}} +$$

$$\frac{1}{m_{A_i}} \sum_{D_k=1}^{N_D} -\nabla[-k_{obj} r_{A_i G}] \frac{(y_{A_i} - y_G)}{r_{A_i G}} + (\alpha_{A_i} - \beta_{A_i} |\vec{v}_{A_i}|^2) \vec{v}_{A_i}$$

$$\frac{\partial x_{A_i}}{\partial t} = v_{A_i,x} \quad (29)$$

$$\frac{\partial y_{A_i}}{\partial t} = v_{A_i,y} \quad (30)$$

$$\frac{\partial^2 x_{D_i}}{\partial t^2} = \frac{1}{m_{D_i}} \sum_{\substack{D_k=1 \\ D_k \neq D_i}}^{N_D} \left[-\frac{C_D}{l_D} e^{-\frac{|r_{D_i D_k}|}{l_D}} + e^{-|r_{D_i D_k}|} \right] \frac{(x_{D_i} - x_{D_k})}{r_{D_i D_k}} \quad (31)$$

$$+ \frac{1}{m_{D_i}} \sum_{D_j=1}^{N_A} -\nabla[-k_{obj} r_{D_i A_j}^{-2}] \frac{(x_{D_i} - x_{A_j})}{r_{D_i A_j}} +$$

$$\left[-\frac{C_{DG}}{l_{DG}} e^{-\frac{|r_{D_i G}|}{l_{DG}}} + e^{-|r_{D_i G}|} \right] \frac{(x_{D_i} - x_G)}{r_{D_i G}} + (\alpha_{D_i} - \beta_{D_i} |\vec{V}_{D_i}|^2) \vec{V}_{D_i}$$

$$\frac{\partial^2 y_{D_i}}{\partial t^2} = \frac{1}{m_{D_i}} \sum_{\substack{D_j=1 \\ D_j \neq D_k}}^{N_D} \left[-\frac{C_D}{l_D} e^{-\frac{|r_{D_i} r_{D_k}|}{l}} + e^{-r_{D_i} r_{D_k}} \right] \frac{(y_{A_i} - y_{A_k})}{r_{D_i} r_{D_k}} + \frac{1}{m_{D_i}} \sum_{D_i=1}^{N_A} -\nabla[-k_{obj} r_{D_i, A_j}^{-2}] \frac{(y_{D_i} - y_{A_j})}{r_{D_i, A_j}} + \left[-\frac{C_{DG}}{l_{DG}} e^{-\frac{|r_{D_i} r_{G}|}{l_{DG}}} + e^{-|r_{D_i} r_{G}|} \right] \frac{(y_{D_i} - y_G)}{r_{D_i, G}} + (\alpha_D - \beta_D |\vec{V}_{D_i}|^2) V_{D_i, y}$$

(32)

$$\frac{\partial x_{D_i}}{\partial t} = v_{D_i, x}$$

(33)

$$\frac{\partial y_{D_i}}{\partial t} = v_{D_i, y}$$

(34)

Eqns. (14) through (21) are the scalar version of the Governing Eqns. (1) to (4), as presented in this paper. They are subjected to known initial conditions: $(v_{A_i, x}, v_{A_i, y}), (x_{A_i}, y_{A_i}), (v_{D_j, x}, v_{D_j, y}), (x_{D_j}, y_{D_j})$ i.e., initial positions and velocities for every individual agent in both the swarms. The Governing Equations are solved using a 4th Order Runge-Kutta method, as outlined in section 2.2 of the paper.

[1] V. Selvi and R. Umarani, International Journal of Computer Applications **5**, 1 (2010).
 [2] C. Carere, S. Montanino, F. Moreschini, F. Zoratto, F. Chiarotti, D. Santucci, and E. Alleva, Animal Behaviour **77**, 101 (2009).
 [3] D. S. Calovi, U. Lopez, S. Ngo, C. Sire, H. Chaté, and G. Theraulaz, New journal of Physics **16**, 015026 (2014).
 [4] M. Moussaid, S. Garnier, G. Theraulaz, and D. Helbing, Topics in Cognitive Science **1**, 469 (2009).
 [5] S. V. Viscido, M. Miller, and D. S. Wethey, Journal of Theoretical Biology **208**, 315 (2001).
 [6] R. Escobedo, C. Muro, L. Spector, and R. Coppinger, Journal of the Royal Society Interface **11**, 20140204 (2014).
 [7] A. Bürkle, F. Segor, and M. Kollmann, Journal of intelligent & robotic systems **61**, 339 (2011).
 [8] M. M. al-Rifaie, A. Aber, and R. Raisys, (2011).
 [9] L. Perea, G. Gómez, and P. Elosegui, Journal of guidance, control, and dynamics **32**, 527 (2009).
 [10] C. W. Reynolds, in *ACM SIGGRAPH computer graphics* (ACM, 1987), pp. 25.
 [11] C. W. Reynolds, in *Game developers conference* (Citeseer, 1999), pp. 763.
 [12] A. Huth and C. Wissel, Ecological modelling **75**, 135 (1994).
 [13] T. Vicsek, A. Czirók, E. Ben-Jacob, I. Cohen, and O. Shochet, Physical review letters **75**, 1226 (1995).
 [14] M. Janosov, C. Virágh, G. Vásárhelyi, and T. Vicsek, New Journal of Physics **19**, 053003 (2017).

[15] M. R. D’Orsogna, Y.-L. Chuang, A. L. Bertozzi, and L. S. Chayes, Physical review letters **96**, 104302 (2006).
 [16] Y.-L. Chuang, M. R. D’orsogna, D. Marthaler, A. L. Bertozzi, and L. S. Chayes, Physica D: Nonlinear Phenomena **232**, 33 (2007).
 [17] A. D. S. Mesa, C. Quesne, and Y. F. Smirnov, Journal of Physics A: Mathematical and General **31**, 321 (1998).
 [18] F. Vecil, P. Lafitte, and J. R. Linares, Physica D: Nonlinear Phenomena **260**, 127 (2013).
 [19] F. Cucker and S. Smale, IEEE Transactions on automatic control **52**, 852 (2007).
 [20] F. Cucker and J.-G. Dong, IEEE Transactions on Automatic Control **55**, 1238 (2010).
 [21] S. M. Ahn and S.-Y. Ha, Journal of Mathematical Physics **51**, 103301 (2010).
 [22] J. Park, H. J. Kim, and S.-Y. Ha, IEEE Transactions on Automatic Control **55**, 2617 (2010).
 [23] S.-Y. Ha, T. Ha, and J.-H. Kim, IEEE Transactions on Automatic Control **55**, 1679 (2010).
 [24] I. Bailey, J. P. Myatt, and A. M. Wilson, Behavioral Ecology and Sociobiology **67**, 1 (2013).
 [25] C. B. Stanford, Animal Behaviour **49**, 577 (1995).
 [26] D. Scheel, Behavioral Ecology **4**, 90 (1993).
 [27] R. L. Vaughn, D. E. Shelton, L. L. Timm, L. A. Watson, and B. Würsig, New Zealand Journal of Marine and Freshwater Research **41**, 391 (2007).
 [28] L. Nøttestad, A. Fernö, and B. E. Axelsen, Polar Biology **25**, 939 (2002).
 [29] L. Angelani, Physical review letters **109**, 118104 (2012).
 [30] Y. Lin and N. Abaid, Physical Review E **88**, 062724 (2013).
 [31] A. Kamimura and T. Ohira, New Journal of Physics **12**, 053013 (2010).
 [32] X. Wang, M. He, and Y. Kang, Physica A: Statistical Mechanics and its Applications **391**, 664 (2012).
 [33] U. Gaertner, UAV swarm tactics: an agent-based simulation and Markov process analysis, 2013.
 [34] S. Luke, George Mason University **1** (2011).
 [35] L. Strickland, M. A. Day, K. DeMarco, E. Squires, and C. Pippin, in *Ground/Air Multisensor Interoperability, Integration, and Networking for Persistent ISR IX* (International Society for Optics and Photonics, 2018), p. 106350Y.
 [36] V. Zhdankin and J. Sprott, Physical Review E **82**, 056209 (2010).
 [37] C. Kolon and I. B. Schwartz, arXiv preprint arXiv:1803.08817 (2018).
 [38] H. E. Espitia and J. I. Sofrony, in *2011 IEEE Congress of Evolutionary Computation (CEC)* (IEEE, 2011), pp. 123.
 [39] J. Rayleigh, (London, 1877).
 [40] H. Gould and J. Tobochnik, *An Introduction to Computer Simulation Methods: Applications to Physical Systems* (Addison-Wesley, 1996).

ADVERSARIAL SWARMS AS DYNAMICAL SYSTEMS

- [41] E. I. Atanassov, (Springer Berlin Heidelberg, Berlin, Heidelberg, 2003), pp. 83.
 - [42] A. Wolf, J. B. Swift, H. L. Swinney, and J. A. Vastano, *Physica D: Nonlinear Phenomena* **16**, 285 (1985).
 - [43] Y. Chen and H. Yang, *Chaos, Solitons & Fractals* **45**, 978 (2012).
 - [44] M. U. Ahmed and D. P. Mandic, *Physical Review E* **84**, 061918 (2011).
 - [45] M. Costa, A. L. Goldberger, and C.-K. Peng, *Physical review E* **71**, 021906 (2005).
 - [46] C. Grebogi, E. Ott, and J. A. Yorke, *Physica D: Nonlinear Phenomena* **7**, 181 (1983).
 - [47] M. Mitchell, P. Hrabar, and J. P. Crutchfield, arXiv preprint [adap-org/9303003](https://arxiv.org/abs/1906.03186) (1993).
 - [48] J. P. Crutchfield, *Nature Physics* **8**, 17 (2012).
 - [49] T. L. Carroll, arXiv preprint [arXiv:1906.03186](https://arxiv.org/abs/1906.03186) (2019).
-